Extended Data for:

“Leukocyte-epithelial physical contacts mediate interstitial migration in vivo”

Jonathan H. Schrope[1,2,3,4,5], Tanner F Robertson[2,*], Adam Horn[2,*], Jack J Stevens[1,2], Clyde Tinnen[1,2], Julie Rindy[2], Yiran Hou[2,5], Emilie Rochon[2], David J Beebe[1,3,6], Anna Huttenlocher[2,5,#]

[1]Department of Biomedical Engineering, University of Wisconsin-Madison, Madison, WI, USA.
[2]Department of Medical Microbiology and Immunology, University of Wisconsin-Madison, Madison, WI, USA.
[3]Department of Pathology and Laboratory Medicine, University of Wisconsin-Madison, Madison, WI, USA.
[4]Medical Scientist Training Program, University of Wisconsin-Madison, Madison, WI, USA.
[5]Department of Pediatrics, University of Wisconsin-Madison, Madison, WI, USA.
[6]Carbone Cancer Center, University of Wisconsin-Madison, Madison, WI, USA.

* These authors contributed equally to this work
[#]Corresponding author: Anna Huttenlocher; huttenlocher@wisc.edu

Previous studies have characterized the anatomy of the larval zebrafish skin, consisting of an epidermal bi-layer composed of superficial and basal keratinocytes, and a deeper matrix-dominated sub-epithelial layer. From live imaging experiments of fish labeling neutrophils (mpx:mCherry) and basal keratinocytes (krtt1c19e:acGFP), we find that neutrophils distribute evenly within both the epithelial (between basal keratinocytes) and sub-epithelial layers (**Extended Data Fig. 1a**). To confirm lower cellularity in the sub-epithelial layer, we fixed larval fish (3 dpf) labeling laminin (lamc1:lamc1-sfGFP) and stained with Hoechst which labels all cell nuclei. Confocal imaging revealed decreased Hoechst signal in the sub-epithelial layer compared to the epithelium (**Extended Data Fig. 1b**). In an orthogonal approach, we also fixed fish labeling the basal epithelial layer (krtt1c19e:acGFP) and stained with Alexa Fluor 594-phalloidin which labels F-actin (**Extended Data Fig. 1c**). Similarly, confocal z-stack images revealed decreased phalloidin signal within the sub-epithelial layer compared to the basal epithelium (**Extended Data Fig. 1d**). Altogether, these data indicate that neutrophils reside in an equal distribution in a cell-dense epithelial layer and cell sparse sub-epithelial layer.

We next sought to quantify differences in neutrophil morphology within these distinct (cellular vs. matrix rich) compartments. Three-dimensional confocal reconstructions of neutrophils in both compartments were generated in Imaris (**Fig S1e, Supplemental Video 1**). This revealed that neutrophils in the epithelium extend a greater number of protrusions (**Fig S1g**) and are less spherical (**Fig S1h**) compared to those in the sub-epithelium.

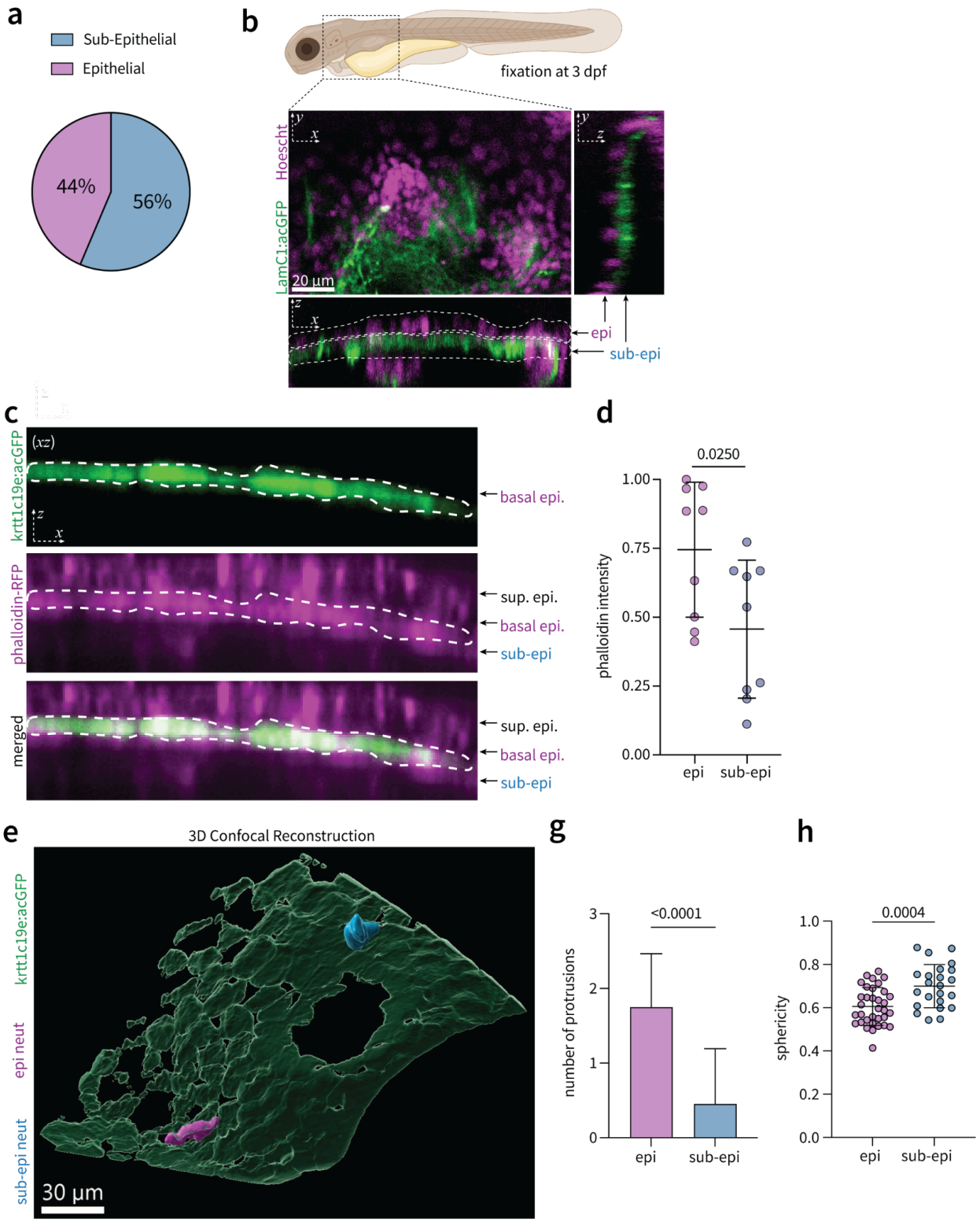

Extended Data Fig. 1. Neutrophils populate distinct tissue environments which regulate cell morphology. a) The proportion of neutrophils inhabiting the epithelial (magenta) vs sub-epithelial (blue) compartments at three days post fertilization (dpf). *P*-value determined by a binomial test with an expected value of .5 (50%). **b)** Representative multi-view confocal image

of fish (Cdh1:Cdh1-sfGFP*)* labeling the laminin-rich sub-epithelial layer, fixed and stained with Hoechst to label cell nuclei. **c)** Representative multi-view confocal image of fish (krtt1c19:acGFP*)* labeling the basal epithelium, fixed and stained with Alexa Fluor 594-phalloidin to label F-actin. Dashed white line indicates the basal epithelial layer. **d)** Quantification of phalloidin signal in the epithelial and sub-epithelial layers; data points indicate mean intensity from single images (n = 9), pooled evenly over three independent experimental replicates. *P*-value determined by two-sample t-test assuming equal variance. **e)** Three-dimensional confocal reconstruction rendered in Imaris depicting neutrophils (mpx:mCherry) populating the epithelial layer (pseudocolored magenta) and sub-epithelial (pseudocolored blue) compartment. **g-h)** Quantification of cell protrusions and sphericity (surface area to volume ratio); each data point represents an individual cell, pooled over three independent experimental replicates. *P*-value determined by two-sample t-test assuming equal variance.

During intra-epithelial migration, surrounding basal keratinocytes act as physical barriers which force decisions of migration path and mechanically confine migratory neutrophils (**Supplemental Video 2)**. Faced with migration path decisions, neutrophils elect the path requiring lesser reorientation of the cell body with respect to the incoming path (**Extended Data Fig. 2a**). Migration path can therefore be predicted at ~ 80% accuracy given prior knowledge of tissue architecture (**Extended Data Fig. 2b**). Given recent findings that the cell nucleus regulates decision making down the path of lesser hydraulic resistance[1], we quantified nuclear shape and positioning during the decision making and passage phases. Nuclear width decreases during the passage phase, and becomes further rearward oriented, consistent with a limiting role of the cell nucleus during confined motility in vivo (**Extended Data Fig. 2c-d, Supplemental Video 3**). During the passage phase, neutrophils must therefore exert expansive forces to deform surrounding epithelial cells (**Extended Data Fig.2e, Supplemental Video 4**).

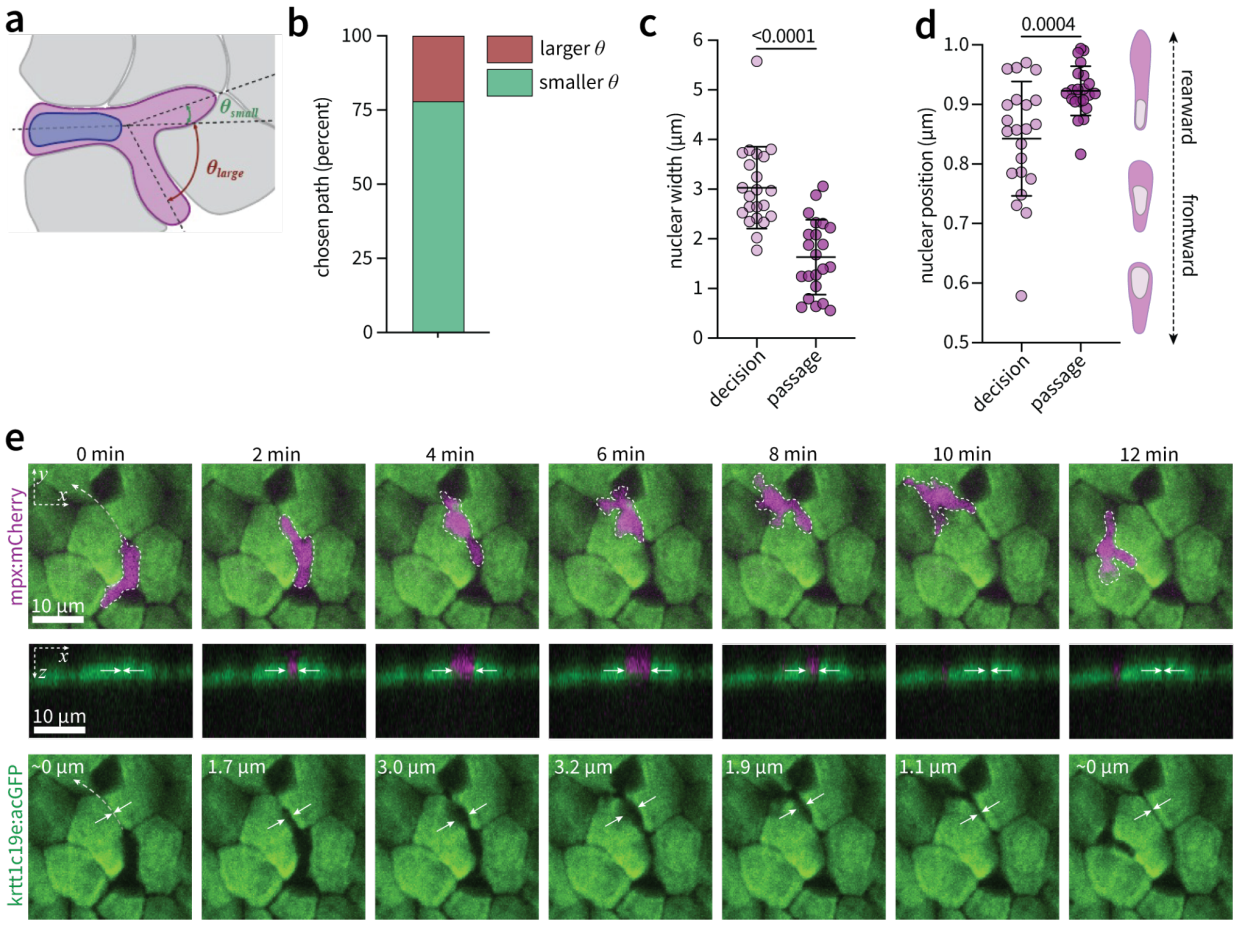

Extended Data Fig. 2. Nuclear positioning during decision making and passage phases. **a)** Schematic depicting potential migration paths during intra-epithelial neutrophil migration, characterized by distinct angles (θ) relative to the incoming path of the cell body. Grey indicates basal keratinocytes, magenta cell cytoplasm, and blue the cell nucleus. **b)** Quantification of chosen paths based on differences in angle relative to incoming path (n = 22 cells pooled over 3 independent zebrafish experiments), *P*-value determined by binomial test with an expected value of .5 (50%). **c-d)** Quantification of nuclear width (c) and positioning (defined as ratio of cell length to the distance between cell front and nucleus rear) (d). Data points represent single cells, pooled over three experimental replicates; *P*-value determined by two-sample *t*-test assuming equal variance. **e)** Maximum intensity *z*-stack projections depicting neutrophil interaction with, and deformation of surrounding keratinocytes. White text (bottom panel) denotes width between keratinocytes during neutrophil passage.

Actin polymerization at the leading edge plays an essential role in exerting expansive forces at the cell front during migration and therefore defines cell polarity when faced with directional decisions of migration path. We therefore sought to characterize F-actin dynamics throughout the decision-making process. At a decision point, neutrophils extend actin-rich protrusions down both potential paths, followed by retraction of the “losing” protrusion (**Extended Data Fig. 3a**) down the path of requiring greater deflection, defined by epithelial tissue architecture. The decision-making step is slow, followed by rapid passage between surrounding basal keratinocytes (**Extended Data Fig. 3a-b**). LifeAct intensity is equal in both protrusions until late throughout the decision-making process, following rapid retraction of the losing arm resulting in a population of central and then rearward actin (**Extended Data Fig. 3d-e**).

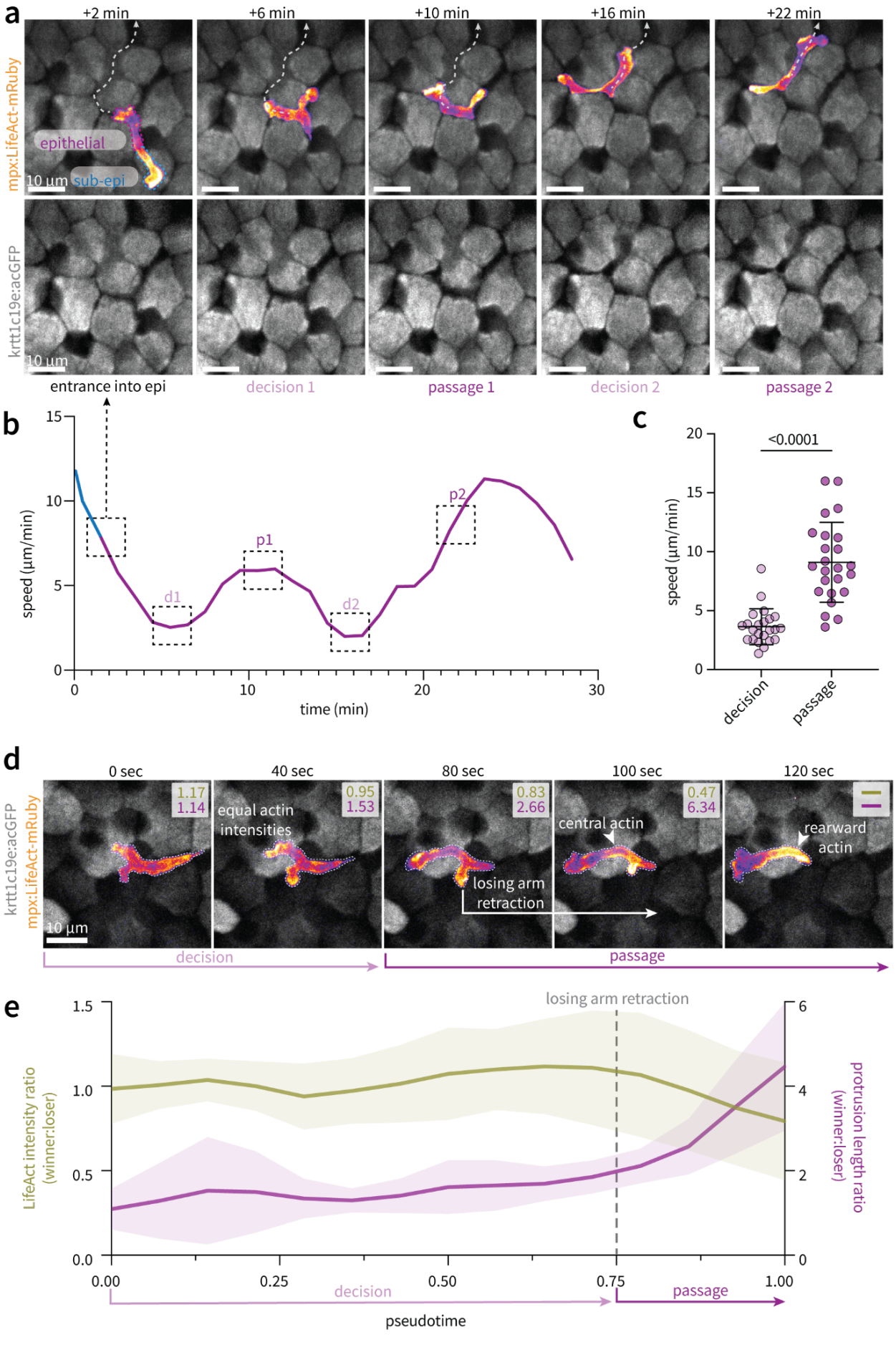
a
+2 min
+6 min
+10 min
+16 min
+22 min
mpx:LifeAct-mRuby
krtt1c19e:acGFP
epithelial
sub-epi
10 µm
entrance into epi
decision 1
passage 1
decision 2
passage 2
b
speed (µm/min)
time (min)
d1
d2
p1
p2
c
<0.0001
speed (µm/min)
decision
passage
d
0 sec
40 sec
80 sec
100 sec
120 sec
1.17
1.14
0.95
1.53
0.83
2.66
0.47
6.34
equal actin intensities
central actin
rearward actin
losing arm retraction
decision
passage
e
losing arm retraction
LifeAct intensity ratio (winner:loser)
protrusion length ratio (winner:loser)
decision
passage
pseudotime

Extended Data Fig. 3. Actin dynamics during decision making. a) Maximum projection z-stack images depicting neutrophil F-actin dynamics (mpx:Lifeact-mRuby) during a decision-making event through basal keratinocytes (krtt1c19e:acGFP, grey). **b-c)** Representative plot (b) and bulk quantification (c) of migration speed during decision-making and passage steps. Data points in (c) represent single cells, pooled over three experimental replicates; *P*-value determined by two-sample *t*-test assuming equal variance. **d)** Maximum intensity z-stack projection images depicting neutrophil F-actin dynamics during decision making and passage phases. **e)** Plot depicting the ratio of LifeAct intensity and protrusion length in the winning and losing arms during decision making (error bars indicate standard deviation of n = 3 decision making events acquired over three independent fish).

To modulate the mechanical resistance exerted by basal keratinocytes during intra-epithelial migration, we leveraged previously reported observations of tissue "fracturing" following focal wounding[2]. Focal laser wounding of basal keratinocytes results in local fracturing near the wound, while minimally impacting the space between keratinocytes in more distant regions (**Extended Data Fig. 4a**). The result is greater space between keratinocytes closer to the wound (**Extended Data Fig. 4b**). Within a ~100 µm distance from the wound site, junctions remain "closed," defined by an epithelial-epithelial cell distance < 1 µm, determined to be the resolution limit of our imaging and quantification protocol.

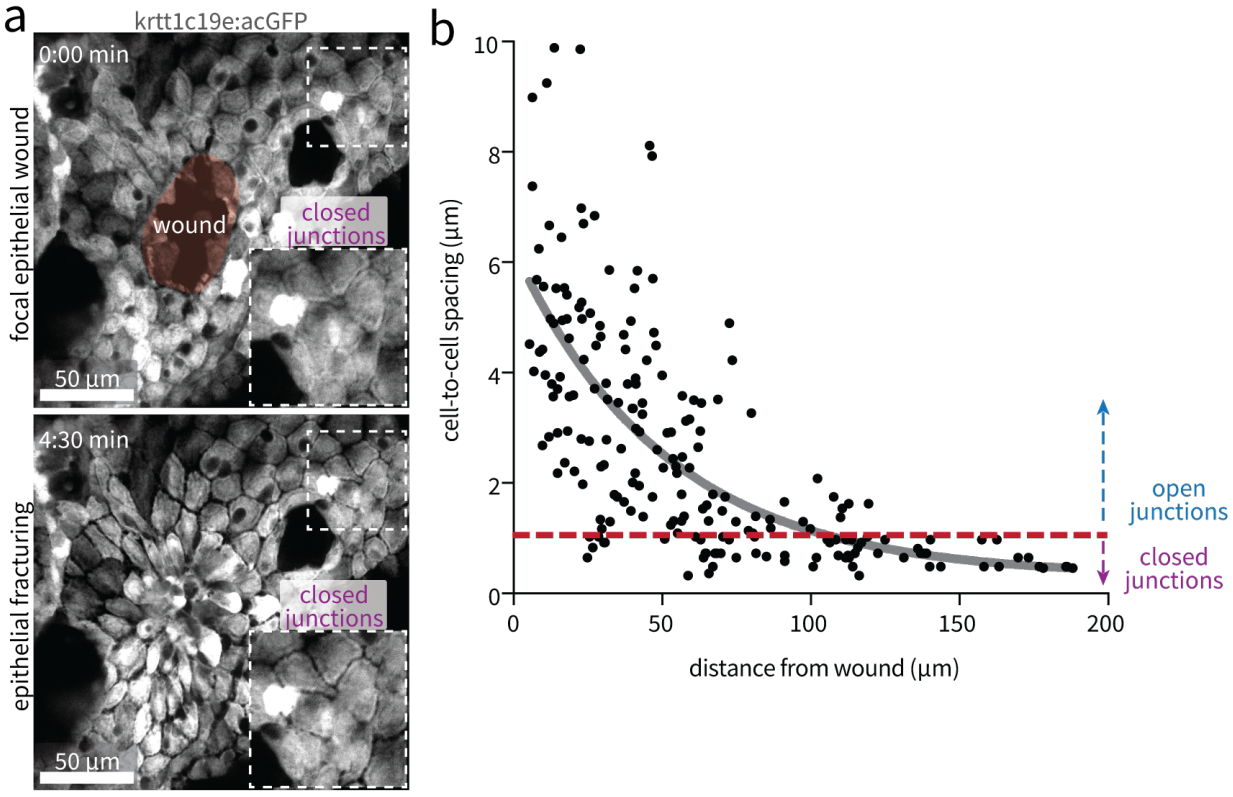

Extended Data Fig. 4. Characterization of epithelial tissue fracturing following focal laser wounding. a) Maximum intensity z-stack projection images depicting spacing between keratinocytes at regions more distant from the focal laser wound site (compare to **Fig 2c** in main text). **b**) Plot of epithelial cell-cell spacing as a function of distance from the wound site. Each

point represents a single epithelial-epithelial spacing measurement, data acquired over 5 independent wounding experiments (n = 80 measurements per each experiment). Closed junctions are defined by spacing < 1 μm, determined to be the resolution limit of the imaging and quantification protocol.

To investigate the regulation of the central actin network, and its requirement for intraepithelial motility, we treated larval fish with Cytochalasin D to inhibit actin polymerization and CK666 to inhibit ARP2/3. Such inhibition of actin abrogated formation of central actin and impaired intra-epithelial motility (**Supplementary Video 5**).

To investigate a role of Cdc42 and WASP in regulating outward pushing forces via the central actin domain, we quantified cell shape under treatment with ZCL278 (Cdc42 inhibitor) or injection with WASP morpholino. We find that both interventions result in cell elongation, quantified by increased aspect ratio (maximum axis divided by minimum axis).

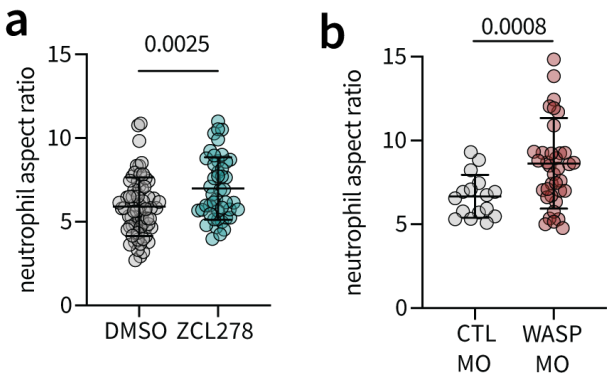

Extended Data Fig. 5. Cdc42 inhibition and WASP knockdown result in neutrophil elongation. a-b) Quantification of cell aspect ratio under treatment with ZCL278 (a) or injection with WASP morpholino (MO) (b). Data points represent single cells, pooled over three experimental replicates; *P*-value determined by two-sample *t*-test assuming equal variance.

Similar to traction force microscopy, which tracks motion of fluorescent markers embedded into elastic matrices in vitro, we sought to utilize the native cluster-like distribution of E-cadherin as surrogate markers to infer forces at the cell-cell (neutrophil-epithelial) interface. This method is contingent upon minimal E-cad cluster displacement in the absence of neutrophil passage. We therefore imaged E-cadherin (Cdh1:Cdh1-YFP) cluster dynamics in regions absent of neutrophils. This revealed minimal displacements of E-cad clusters compared to that observed during epithelial-cell interaction with neutrophils (**Extended Data Fig. 6, Fig. 4-5**, **Supplementary Video 5**).

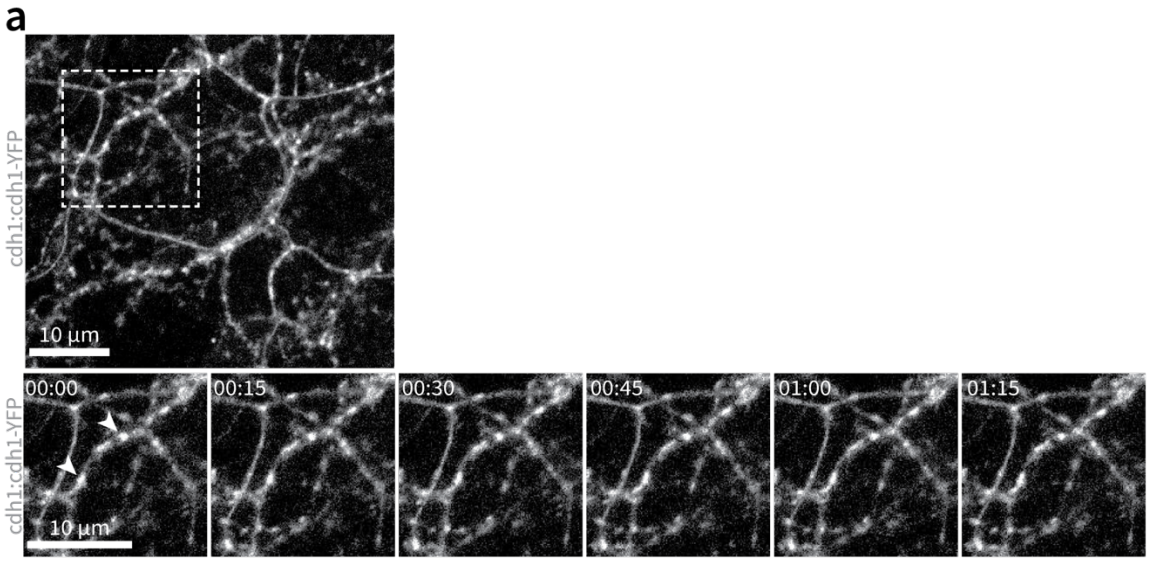

Extended Data Fig. 6. Epithelial cadherin dynamics in basal epithelium in the absence of neutrophil passage. Maximum-intensity projection images depicting E-cad (Cdh1:Cdh1-YFP) cluster dynamics over time. White arrows depict example clusters.

To test the hypothesis that αE integrin-mediated interaction with epithelial cadherin facilitates neutrophil intra-epithelial motility, we performed CRISPR-mediated deletion of αE integrin in larval zebrafish. Zebrafish underwent a genome duplication early in evolution, resulting in two copies of the integrin αE gene (*itgae.1* and *itgae.2*). To identify neutrophil expression levels of both genes, we compared expression levels of both genes to the neutrophil specific *mpx* gene, within publicly available single-cell sequencing data of larval zebrafish available through ZebraHub. This revealed that neutrophils do not express *itgae.1*, but do express *itgae.2* (**Fig S7**). Instead, *itgae.1* is more highly expressed in macrophages (expressing *mpeg1.1*)

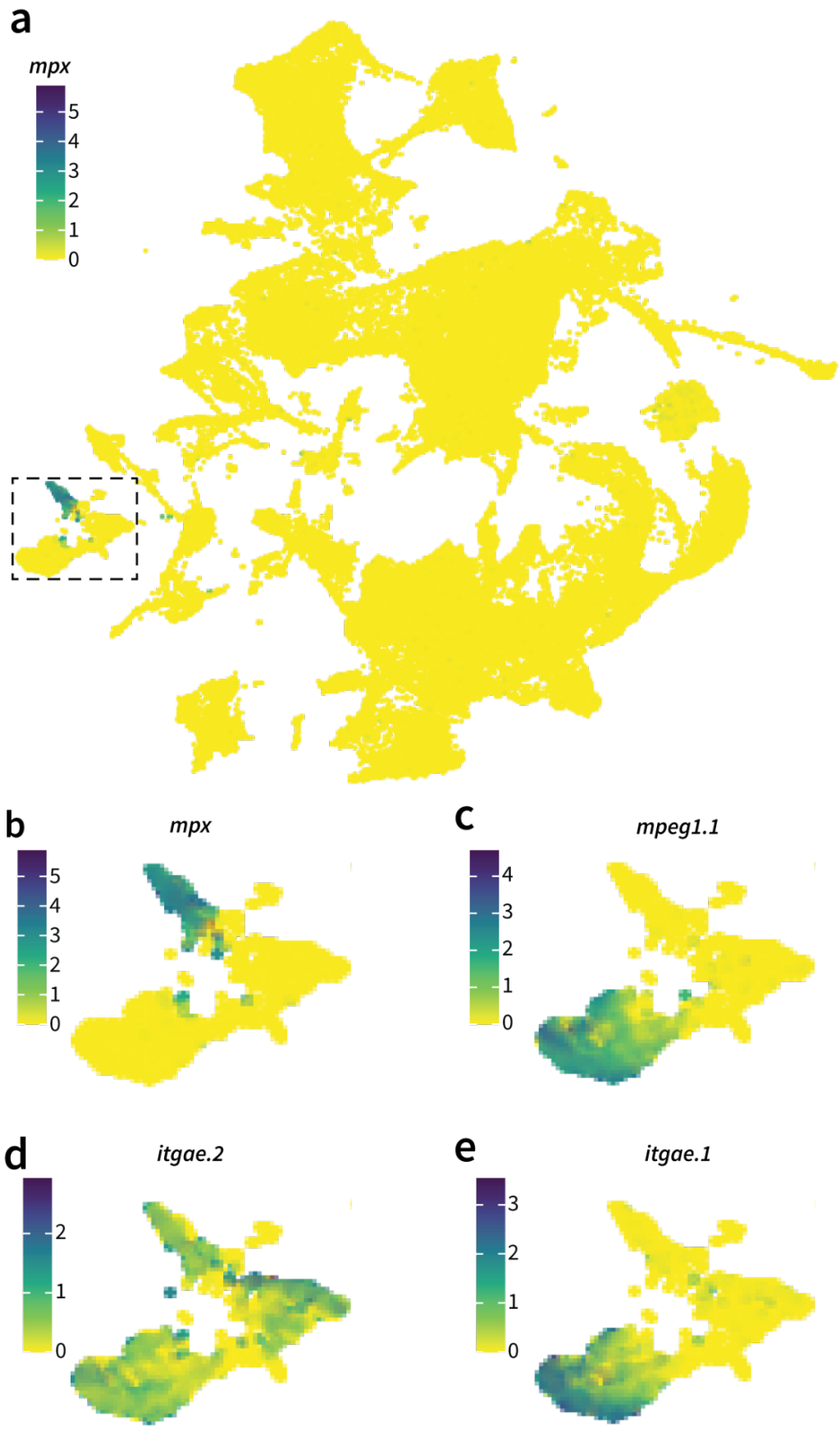
a
mpx
5
4
3
2
1
0
b
mpx
5
4
3
2
1
0
c
mpeg1.1
4
3
2
1
0
d
itgae.2
2
1
0
e
itgae.1
3
2
1
0

Extended Data Fig. 7. Expression of integrin αE (*itgae*) genes in neutrophils and macrophages. a) Uniform Manifold Approximation and Projection (UMAP) depicting single cell expression landscape in larval zebrafish with color indicating normalized expression level of the neutrophil-specific *mpx* gene. The dashed black box denotes the cluster corresponding to leukocytes. **b-e)** Inserts of leukocyte clusters with expression of *mpx* (neutrophils) (b), *mpeg1.1* (macrophages) (c), *itgae.2* (d), and *itgae.1* (e).

In addition to quantifying αE integrin-E-cadherin-mediated traction forces (**Fig. 5** in main text), we also sought to explore whether αE integrin regulated formation of the central actin network during passage between surrounding epithelial cells. We find that αE integrin mutants do not exhibit significant differences in the ratio of central to leading edge actin (**Fig S8c**), cell elongation (**Fig S8d**), or deformation of surrounding epithelial cells (**Fig S8e**).

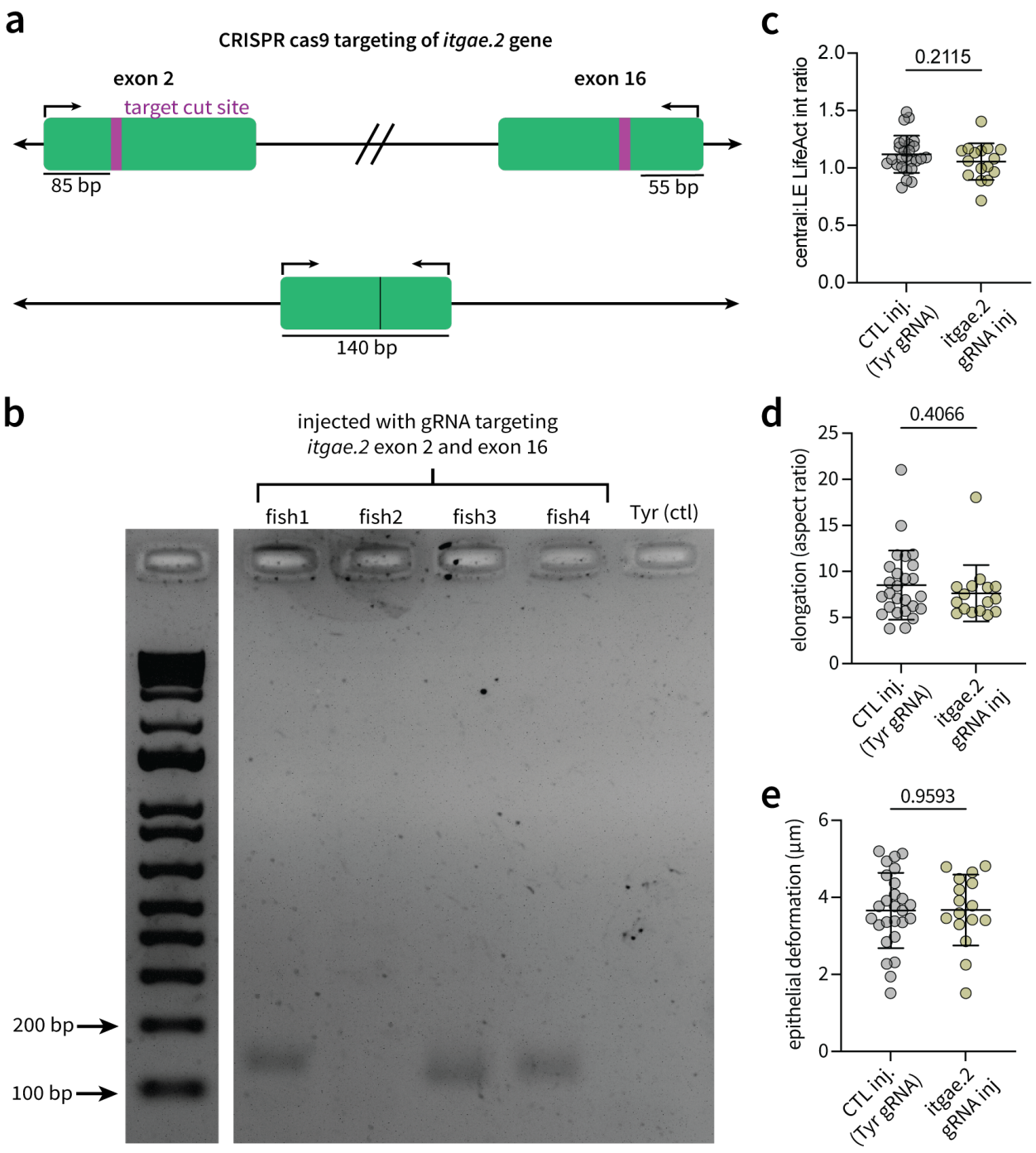

Extended Data Fig. 8. CRISPR experimental design and *itgae.2* regulation of central actin. **a)** Schematic depicting gRNA targeting strategy and expected result, confirmed by sequencing **b**) PCR product gel electrophoresis of four *itgae.2* gRNA injected fish and a control (tyrosinase-targeting) injected fish. Fish 1,3,4 have a band at ~140 bp indicating successful deletion of ~5500 bp region of the gene, confirmed by sequencing. **c-e**) Quantification of the ratio between central actin (middle third) and leading-edge actin (front third) (c), cell elongation determined by aspect ratio (d), and epithelial deformations (e), following injection with guide RNA targeting

itgae.2 versus tyrosinase (control). Data points represent single cells, pooled over three experimental replicates; *P*-value determined by two-sample *t*-test assuming equal variance.